arXiv:physics/0509069v1 [physics.plasm-ph] 8 Sep 2005

On the inverse cascade of magnetic helicity

Alexandros Alexakis,* Pablo Mininni,† and Annick Pouquet‡
National Center for Atmospheric Research
(Dated: February 2, 2008)

We study the inverse cascade of magnetic helicity in conducting fluids by investigating the detailed transfer of helicity between different spherical shells in Fourier space in direct numerical simulations of three-dimensional magnetohydrodynamics (MHD). Two different numerical simulations are used, one where the system is forced with an electromotive force in the induction equation, and one in which the system is forced mechanically with an ABC flow and the magnetic field is solely sustained by a dynamo action. The magnetic helicity cascade at the initial stages of both simulations is observed to be inverse and local (in scale space) in the large scales, and direct and local in the small scales. When saturation is approached most of the helicity is concentrated in the large scales and the cascade is non-local. Helicity is transfered directly from the forced scales to the largest scales. At the same time, a smaller in amplitude direct cascade is observed from the largest scale to small scales.

PACS numbers: 47.65.+a; 47.27.Gs; 95.30.Qd

I. INTRODUCTION

The generation of magnetic fields in various astrophysical objects ranging from planets (e.g. the geodynamo [1, 2]), to stars (e.g the solar dynamo [3, 4, 5]), and spiral galaxies (e.g. the interstellar dynamo [6]), is mostly attributed to dynamo action due to motions of a conducting fluid [7]. Due to the magnetic flux conservation in ideal magnetohydrodynamics (MHD), the stretching of magnetic field lines by a conducting flow amplifies the magnetic energy at small scales. To further explain how magnetic fields end up in scales much larger than the outer scales of fluid motions, one of the theoretical arguments used is the inverse cascade of magnetic helicity in MHD turbulence. It is worth mentioning here that the the presence of helicity in the flow, although helpful, is not required to generate large scale magnetic fields. In some circumstances, large scale fields can be sustained solely by helicity fluctuations [8], by anisotropic flows [9], or large scale shear [10].

Early studies using mean-field theory [11, 12] and turbulent closure models [13, 14] have shown within the framework of the approximations made that magnetic helicity cascades inversely from small scales to large scales. Direct numerical simulations (DNS) [15, 16, 17, 18, 19] have verified the inverse cascade of magnetic helicity and have shown the generation of large scale magnetic fields from small scale helical forcing. A detailed examination of the cascading process was investigated in [18], where the rate of transfer of magnetic energy among different scales was measured from DNS. The results showed evidence of nonlocal energy transfer of magnetic energy from the small scales to the large scales, suggesting also a nonlocal transfer of magnetic helicity. However, in three dimensional MHD turbulence the ideal invariant that can display an inverse cascade, *stricto sensu*, is the magnetic helicity, not the magnetic energy, and no direct attempt to measure its transfer in simulations has been done so far.

In this paper we focus on helical flows, and revisit the problem of the inverse cascade of the magnetic helicity by analyzing two DNS: one forced through the induction equation by an external electromotive force, and one forced mechanically. In both simulations, the forcing was applied in small scales so that enough large scales were available for an inverse cascade to develop. Note that this election naturally limits the Reynolds numbers we can resolve, and as a result only moderate Reynolds numbers will be considered in this work. Extending the formalism used in [20, 21, 22, 23] for the transfer of the magnetic and kinetic energy, we directly measured the transfer rate of magnetic helicity among different scales, both in scales larger and smaller than the forcing scales.

The outline of the paper is as follows. In Sec. II we present a brief review of the equations and definition of transfer functions needed to study this problem. In Sec. III we give the results from the magnetically forced simulation; and in Sec. IV we give the results from the mechanically forced simulation. Finally, we discuss the implications of our results in Sec. V, where we also give our conclusions.

II. THEORY AND DEFINITIONS

To a good approximation the equations that describe the dynamics of an incompressible conducting fluid coupled to a magnetic field are given by:

$$\partial_t \mathbf{u} + \mathbf{u}\cdot\nabla\mathbf{u} = -\nabla P + \mathbf{b}\cdot\nabla\mathbf{b} + \nu\nabla^2\mathbf{u} + \mathbf{f} \qquad (1)$$

$$\partial_t \mathbf{b} = \nabla\times(\mathbf{u}\times\mathbf{b}) + \eta\nabla^2\mathbf{b} + \nabla\times\mathbf{E} \qquad (2)$$

*Electronic address: alexakis@ucar.edu
†Electronic address: mininni@ucar.edu
‡Electronic address: pouquet@ucar.edu

where $\mathbf{u}$ is the velocity field, $\mathbf{b}$ is the magnetic field, ν is the kinematic viscosity, η is the magnetic diffusivity, P is the total pressure, $\mathbf{f}$ an external mechanic force, and $\mathbf{E}$ is an external electromotive force. The equations are written in the familiar Alfvénic dimensionless units. These equations are accompanied by the conditions $\nabla \cdot \mathbf{u} = 0 = \nabla \cdot \mathbf{b}$. This last condition allows us to write the magnetic field in terms of a vector potential $\mathbf{b} = \nabla \times \mathbf{a}$. Removing a curl from Eq. (2), the evolution equation for the vector potential reads:

$$\partial_t \mathbf{a} = \mathbf{u} \times \mathbf{b} + \eta \nabla^2 \mathbf{a} - \nabla \phi + \mathbf{E} \tag{3}$$

where the Coulomb gauge ($\nabla \cdot \mathbf{a} = 0$) is assumed and $\nabla\phi$ is determined by the solenoidal condition on $\mathbf{a}$. There are three quadratic invariants in the absence of dissipation and forcing: the total energy $E = \int (\mathbf{b^2} + \mathbf{u^2})/2 \, dx^3$, the cross-helicity $H_c = \int \mathbf{b} \cdot \mathbf{u} \, dx^3$, and the magnetic helicity $H_m = \int \mathbf{b} \cdot \mathbf{a}/2 \, dx^3$. To the best of our knowledge the magnetic helicity, which is the quantity under investigation in this paper, was first introduced as an invariant of the MHD equations by Woltjer [24]. It is proportional to the number of linkages of the magnetic field lines [7], as is reflected by its relation with topological quantities as the Gauss linking number [25, 26]. The conservation of magnetic helicity is related with the frozen-in theorem of Alfvén. Being magnetic field lines material, a link can only change through reconnection of field lines, and therefore breaking of the frozen-in condition (*e.g.* through dissipation) is needed.

As we stated in the introduction, we want to quantify the rate at which helicity is transfered among the different scales of the magnetic field. To define the magnetic field and vector potential at different scales, we introduce the shell-filtered magnetic field and vector potential components $\mathbf{b}_K(\mathbf{x})$ and $\mathbf{a}_K(\mathbf{x})$. Here, the subscript K indicates that the field has been filtered to keep only the modes whose wave vectors are in the Fourier shell $[K, K+1]$ (hereafter called the shell K). Clearly the sum of all the K components gives back the original field, $\mathbf{b} = \sum_K \mathbf{b}_K$, and the filtering operation commutes with the curl operator, $\nabla \times \mathbf{a}_K = \mathbf{b}_K$. A similar decomposition has been used in [22, 23] to study the cascade of energy.

We are interested in the rate that magnetic helicity at a given shell Q is transferred into a different shell K. From the MHD equations, taking the dot product of Eq. (3) with $\mathbf{b}_K/2$, taking the dot product of Eq. (2) with $\mathbf{a}_K/2$, adding them, and integrating over space, we finally obtain the evolution of the magnetic helicity $H_m(K) = \frac{1}{2}\int \mathbf{a}_K \cdot \mathbf{b}_K \, dx^3$ in the shell K:

$$\partial_t H_m(K) = \sum_Q \int \mathbf{b}_K \cdot (\mathbf{u} \times \mathbf{b}_Q) \, d\mathbf{x}^3 - \\ - \eta \int \mathbf{b}_K \cdot \nabla \times \mathbf{b}_K \, d\mathbf{x}^3 + \int \mathbf{b}_K \cdot \mathbf{E}_K \, d\mathbf{x}^3 \ . \tag{4}$$

We can rewrite Eq. (4) in a more compact form

$$\partial_t H_m(K) = \sum_Q \mathcal{T}_h(K,Q) - \eta \mathcal{D}_h(K) + \mathcal{F}_h(K), \tag{5}$$

where we have introduced the transfer function $\mathcal{T}_h(Q,K)$, the helicity injection $\mathcal{F}_h(K)$, and the helicity dissipation $\mathcal{D}_h(K)$ as defined below.

The dissipation of magnetic helicity in the shell K is given by

$$\mathcal{D}_h(K) = \int \mathbf{b}_K \cdot (\nabla \times \mathbf{b}_K) d\mathbf{x}^3, \tag{6}$$

Note however that unlike the energy dissipation this is not a positive definite quantity.

The injection rate of magnetic helicity in the shell K by the external electromotive force $\mathbf{E}$ is given by

$$\mathcal{F}_h(K) = \int \mathbf{b}_K \cdot \mathbf{E}_K \, d\mathbf{x}^3. \tag{7}$$

Note that the mechanical forcing $\mathbf{f}$ does not inject magnetic helicity in the system, as follows from Eq. (4). However, as will be discussed later, if the external mechanical forcing is helical, the velocity field can generate helical magnetic fields locally through the $\mathcal{T}_h(Q,K)$ term.

The transfer rate of magnetic helicity at shell Q into magnetic helicity at shell K is defined as:

$$\mathcal{T}_h(K,Q) = \int \mathbf{b}_K \cdot (\mathbf{u} \times \mathbf{b}_Q) d\mathbf{x}^3. \tag{8}$$

$\mathcal{T}_h(K,Q)$ expresses the transfer rate of positive helicity from the shell Q to the shell K, or equivalently the transfer rate of negative helicity from the shell K into the shell Q. Positive values of $\mathcal{T}_h(K,Q)$ imply that positive helicity is transfered from the shell Q to the shell K, while negative values imply the reverse transfer. The transfer term is a conservative term and it does not generate or destroy total magnetic helicity. However, this term is responsible for the redistribution of magnetic helicity among different scales. This fact is expressed by the antisymmetry property of $\mathcal{T}_h(Q,K)$:

$$\mathcal{T}_h(K,Q) = -\mathcal{T}_h(Q,K) \ . \tag{9}$$

We stress that helicity (unlike energy) is not a positive definite quantity and care needs to be taken when we interpret results. We will not attempt here a separation of its different sign components (see e.g. [27, 28, 29] for the kinetic helicity in hydrodynamic turbulence). As an example, if in some shell K the helicity is positive $H_b(K) > 0$ with a positive rate of change $\partial_t H_b(K) > 0$, then the magnetic field becomes more helical in that shell as the system evolves. If however the helicity is negative $H_b(K) < 0$, then positive rate of change implies that the field becomes less helical in that shell. In the same spirit, if positive helicity is transfered from scales with negative helicity to scales with positive helicity, the field becomes

more helical at both scales even if the total helicity at all scales remains constant. On the other hand, if positive helicity is transfered from scales with positive helicity to scales with negative helicity, the field becomes less helical at each scale since the absolute value of magnetic helicity in each scale is decreased.

III. MAGNETICALLY FORCED RUN

We begin with the magnetically forced simulations. In this case, a helical ABC electromotive force **E** is used, while keeping the mechanical force equal to zero. The flow evolution is solved using a pseudospectral method with the 2/3-rule for dealiasing on a $N^3 = 256^3$ grid. No uniform magnetic fields is allowed in the periodic box, and therefore magnetic helicity conservation is satisfied in the ideal case [26].

The viscosity and diffusivity are set to $\nu = \eta = 5 \times 10^{-4}$. Only wavenumbers in the shells 8 and 9 are forced. The phase of the external ABC electromotive force is changed randomly with a correlation time $\tau = 1.25 \times 10^{-2}$, and the time step to satisfy the Courant-Friedrichs-Levy (CFL) condition is set to $\Delta t = 2.5 \times 10^{-3}$. The integral lenghtscale of the flow $L = 2\pi \int E(K)/K dk/E$ (where $E(K)$ is the kinetic energy in the shell K, and E is the total kinetic energy) in the steady state of the simulation is $L \approx 1.42$, and the large scale turnover time $T = U/L$ (where U is the r.m.s. velocity) is $T \approx 0.25$. Based on these numbers, the resulting kinetic Reynolds number R_e and magnetic Reynolds number R_m are $R_e \approx R_m \approx 700$. The simulation is well resolved, in the sense that the Kolmogorov's kinetic [$k_\nu = (\epsilon/\nu^3)^{1/4}$, where ϵ is the total energy injection rate] and magnetic [$k_\eta = (\epsilon/\nu^3)^{1/4}$] dissipation wavenumbers are smaller than the maximum resolved wavenumber $k_{max} \approx N/3$.

The magnetically forced case is easier to analyze because only one sign of helicity appears to dominate all scales. In Fig. 1 we show the resulting spectra at two different times t_1 and t_2, up to wavenumber $k = 40$. The former time is early (before the system comes close to saturation), and the latter time is when the flow is almost saturated. Note that the maximum wavenumber in the code is $k_{max} \approx 85$, and the dissipative range in the simulation extends to larger wavenumbers than what is shown in Fig. 1. However, the transfer function $\mathcal{T}_h(K, Q)$ will only be computed up to $K, Q = 40$, a range that includes all scales larger (wavenumbers smaller) than the injection band, as well as the scales smaller than the injection band where a turbulent scaling can still be identified. We will follow this convention in the following figures.

A. Early times

The spectrum of magnetic helicity for $t = t_1$ is shown in Fig. 2(a), in log-log scale and is positive at all scales. At this stage, the magnetically helicity spectrum peaks at

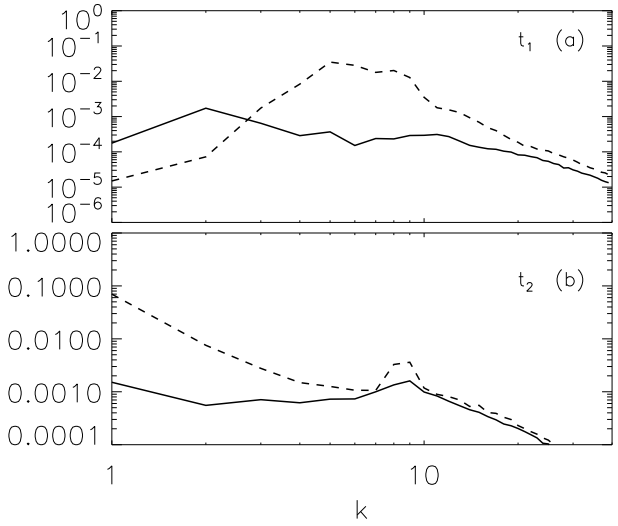

FIG. 1: The kinetic (solid line) and magnetic (dashed line) energy spectra for the magnetically forced simulation and for two different times: panel (a) t_1 before saturation is reached, panel (b) t_2 close to saturation. The figure shows the spectrum up to $k = 40$, note however that the maximum wavenumber resolved in the code is $k_{max} \approx 85$.

wave number $K \simeq 5$, a scale slightly larger than the scale where the system is forced. Panels (b-e) show the transfer of magnetic helicity $\mathcal{T}_h(K, Q)$ at different values of Q, normalized by the total magnetic helicity in that shell. The dotted lines in these panels indicate the shell where the forcing is applied, while the dashed lines indicate the mode that is examined.

Since the helicity is positive for all scales, we only need to interpret $\mathcal{T}_h$ as transfer of positive helicity. In Fig. 2, panel (b) shows the transfer $\mathcal{T}_h(K, Q)$ for wavenumbers at the peak of the energy spectrum ($K = 5$). For smaller wavenumbers ($K < 5$) the transfer is positive, while it is negative for larger wave numbers ($K > 5$). This picture indicates that the shell $K = 5$ is giving/transferring helicity to its close neighbors on the left, while it receives helicity from its neighbors on the right.

Similar behavior is observed for the modes with wavenumbers between the peak of magnetic helicity in Fourier space and the forcing wave number [see panel (a)]. The transfer of magnetic helicity for a value of Q in this range ($Q = 7$) is shown in panel (c), suggesting the picture of a local inverse cascade. Indeed, the shell $Q = 7$ gives most of its helicity to the shell $K \approx 6$ (positive peak), while receives helicity from the shell $K \approx 8$ (negative peak).

The forced wave numbers [the transfer $\mathcal{T}_h(K, Q)$ for $Q = 8$ is shown in panel (d)] are giving helicity to both smaller and larger scales, with a preference towards the larger scales (smaller wave numbers). Finally, wavenumbers larger than the forced scale [panel (e)] have a different behavior. Unlike the large scales, the small scales ($K = 20$ is displayed here) receive helicity from larger scales (but smaller than the forced scale) and give helic-

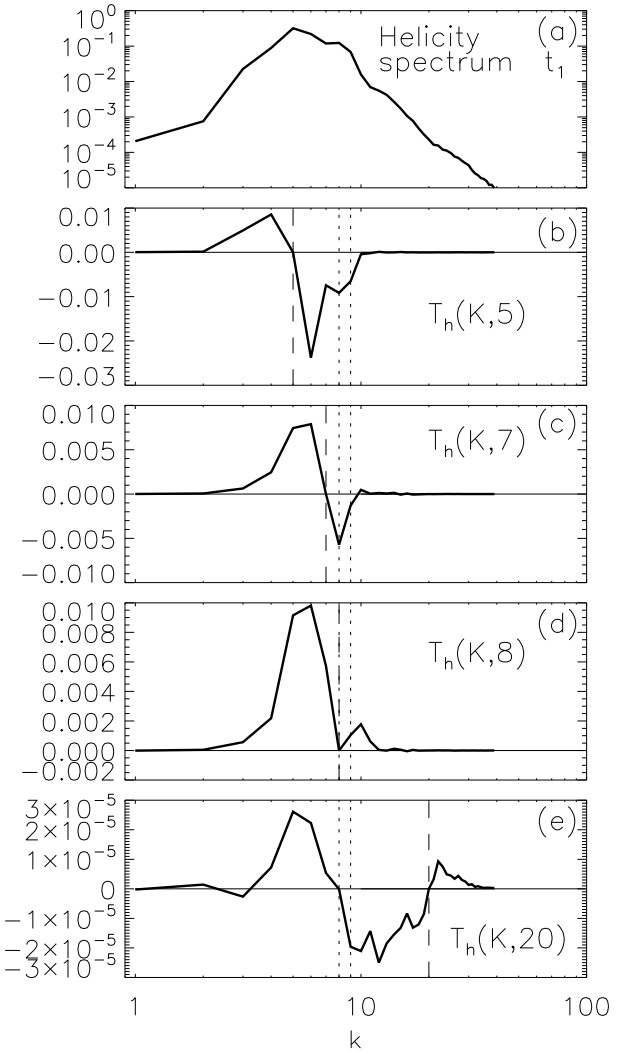

FIG. 2: The magnetic helicity (panel a) and its transfer $\mathcal{T}_h(K,Q)$ from shell Q to shell K,normalized by the total magnetic helicity for the magnetically forced run at time t_1. The different panels (b-e) correspond to different values of $Q = 5, 7, 8, 20$. The dashed vertical line indicates the location of the examined value of Q while the dotted lines give the width of the forcing band. Note that the transfer for $Q = 20$ is significantly smaller.

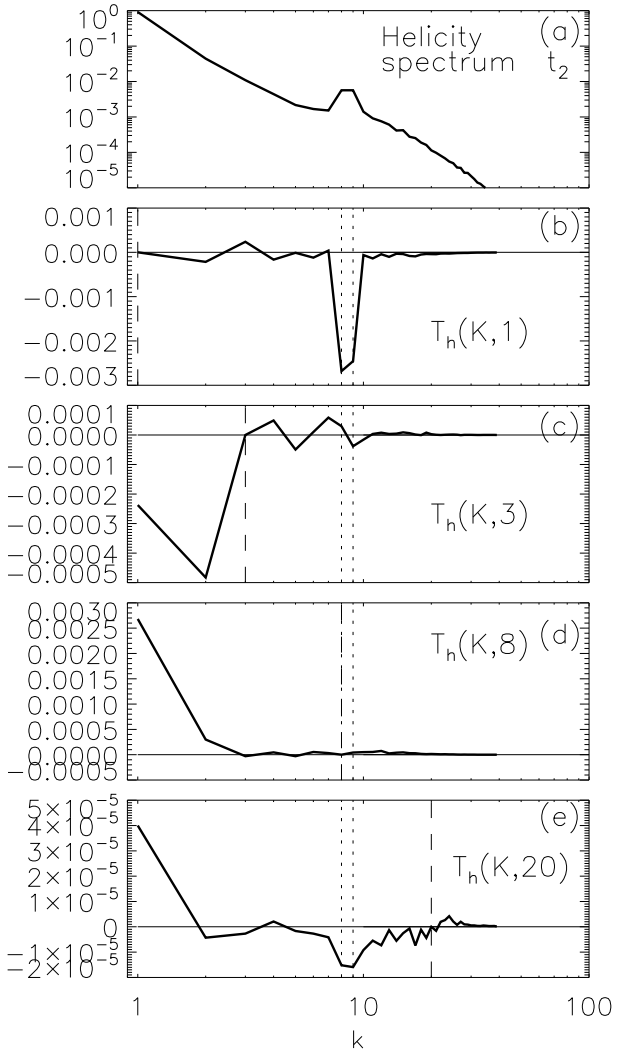

FIG. 3: The magnetic helicity (panel a) and its transfer $T_h(K,Q)$ from shell Q to shell K, normalized by the total magnetic helicity for the magnetically forced run, at later times. The different panels (b-e) correspond to different values of $Q = 1, 3, 8, 20$ The dashed vertical line indicates the location of the examined value of Q while the dotted lines give the width of the forcing band. Note the different values on the vertical axis.

ity to smaller scales. This suggests a local direct cascade of positive magnetic helicity. In addition, there is a non-local transfer of helicity to much larger scales ($K \simeq 5$), probably associated to reconnection events.

B. Late times

The picture of local cascade of helicity is changed at later times, as the peak of the helicity spectrum moves to the largest possible scale ($K = 1$). The helicity spectrum and the transfer functions at this stage are shown in Fig. 3. The helicity spectrum peaks strongly at $K = 1$ [see panel (a)]. As shown in panel (b), the largest scales are now receiving magnetic helicity directly from the forced scales, the remaining scales giving almost zero contribution. This behavior suggests a non-local inverse cascade. Intermediate scales between the largest available and the forced scales have also changed their behavior [panel (c)]. These scales ($1 < K < 8$) now are receiving positive helicity mostly from the largest modes and giving it to the smaller scales. This suggests a direct cascade of positive magnetic helicity in the range $1 < K < 8$. It appears therefore that once the magnetic helicity has reached the largest possible scale there may be some "reflection" at $K = 1$, and helicity then cascades to smaller scales with the exception of the forced modes that continue feeding the magnetic helicity at the largest scale [see panel

(d)]. Scales smaller than the injection band transfer the positive magnetic helicity to smaller scales as at early times, with the exception of a non-local direct input to the largest scale.

The "reflection" of magnetic helicity in Fourier space when it reaches the largest scale in the box, suggests that the late time evolution is strongly dependent on the boundary conditions. In our case, the periodic boundary conditions do not allow magnetic helicity to grow at scales even larger, and forbids the system to eject magnetic helicity outside the box. Similar behavior has been observed in two-dimensional hydrodynamic turbulence, where the quantity which has an inverse cascade is the energy [30, 31, 32]. For this latter problem, evidence of nonlocal and irregular transfer of the inverse cascading invariant was also found in simulations [33]. We will come back to this issue later.

IV. MECHANICALLY FORCED RUN

We move next to the case where the system is mechanically forced, and the magnetic field is solely amplified and sustained against Ohmic dissipation by dynamo action. This case is more relevant to most physical situations. In this case, we perform a numerical simulation using a grid of $N^3 = 256^3$ points under the following procedure. First, a hydrodynamic simulation was performed mechanically forcing at wave number $K = 10$, with an ABC flow to obtain a turbulent steady state. The kinetic helicity of the flow $H_k = \int \mathbf{u} \cdot \nabla \times \mathbf{u}/2 \, d^3x$ in the steady state is positive, and close to maximal. Unlike the previous section, here the phases of the ABC flow are kept constant as a function of time.

After reaching the hydrodynamic steady state, a random, non-helical, and small magnetic field was introduced and the simulation was carried keeping the force fixed to observe the evolution of the system from the initial exponential amplification of the magnetic energy until the large-scale saturation. The kinematic viscosity and magnetic diffusivity were $\eta = \nu = 2.5 \times 10^{-3}$. In the hydrodynamic steady state, the integral scale of the flow was $L \approx 0.6$ and the large scale eddy turnover time $T \approx 0.6$. Based on these numbers, the mechanic and magnetic Reynolds numbers were $R_e = R_m = 240$.

From Eqs. (5) and (7), we note that a helical mechanical force cannot inject net magnetic helicity in the system. However, a flow with positive kinetic helicity in the forcing band generates equal amounts of magnetic helicity at large and small scales with opposite signs. This generation can be understood in a geometrical way from the Stretch Twist -Fold (STF) dynamo [34]. As magnetic flux tubes at large scales are twisted in one direction (generating one sign of magnetic helicity), magnetic field lines at small scales are twisted in the opposite direction.

This generation of opposite signs of magnetic helicity at different scales is also a signature of the α-effect [35]. In mean field theory (see*e.g* [12]) the equation for the evolution of the mean magnetic helicity $\overline{H}_m$ is

$$\partial_t \overline{H}_m = \int \left(\alpha \overline{B}^2 - \beta \overline{\mathbf{B}} \cdot \nabla \times \overline{\mathbf{B}} \right) d^3x. \qquad (10)$$

where $\alpha \approx -\tau \langle \mathbf{v} \cdot \nabla \times \mathbf{v} \rangle$ is proportional to minus the kinetic helicity of the flow (here $\mathbf{v}$ is the fluctuating velocity field, and τ is a correlation time). The coefficient β is a positive turbulent diffusivity. As a result, the α-effect injects magnetic helicity of opposite sign than the kinetic helicity into the mean (large scale) magnetic field. As its counterpart, at small scales the fluctuating magnetic field receives magnetic helicity of the same sign than the kinetic helicity.

We will investigate three different times. In the first case, the dynamo is still kinematic (*i.e.* the magnetic energy is smaller than the kinetic energy at all scales, and the effect of the Lorentz force on the velocity field can thus be neglected). In the second, kinetic and magnetic energies are of the same order but the peak of the magnetic helicity is not at the largest scales yet. In this regime, scales smaller than the energy injection band have reached saturation, while the large scale magnetic field keeps growing slowly. Finally, we investigate the saturated stage where the magnetic helicity spectrum peaks at the largest attainable scale.

The energy spectra for these three cases are shown in Fig. 4. As in the previous section, the maximum wavenumber resolved in the simulation was $k_{max} \approx 85$, and at all times the Kolmogorov's dissipation wavenumbers were smaller than k_{max}. Since the transfer between different shells will only be studied up to $K, Q = 40$, all spectral quantities in the figures are shown up to this wavenumber.

A. Kinematic regime

We begin with the kinematic regime. The magnetic helicity spectrum is shown in Fig. 5(a). Unlike the magnetically forced case, the magnetic helicity spectrum changes sign. For scales smaller than the forced scales, the magnetic helicity spectrum is positive, while at large scales the magnetic helicity is negative. The positive and negative peaks are close on either side of the forced band. The transfer of helicity $\mathcal{T}_h(K, Q)$ for various shells Q is shown in Figs. 5(b-e).

The large scales [$Q = 5$ is shown in panel (b)], where the negative peak of the magnetic helicity spectrum is located, receive some negative helicity from smaller scales, but most of the transfer is from the forced scales ($K \approx 10$). These scales also give (negative) helicity to larger scales [see panels (b) and (c)]. Note that because helicity is negative in the large scales, a positive values of $\mathcal{T}_h(K, Q)$ means that the shell K receives negative magnetic helicity from the shell Q, increasing the absolute value of the magnetic helicity in the shell K, and the other way around if $\mathcal{T}_h(K, Q)$ is negative.

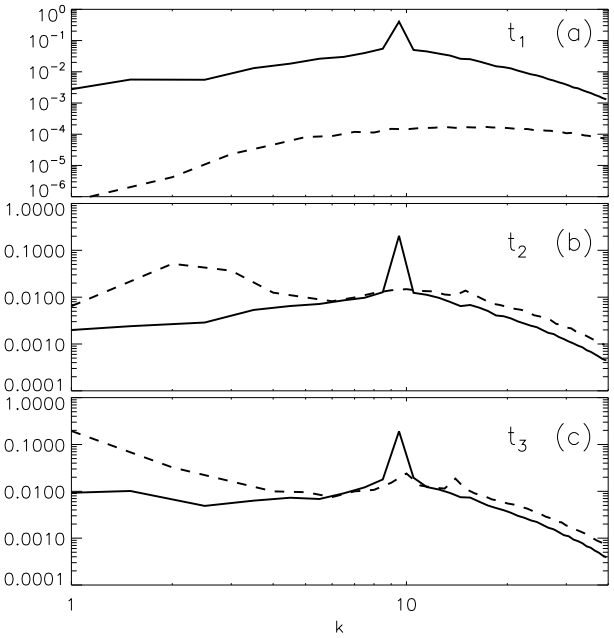

FIG. 4: The kinetic energy spectrum (solid line) and the magnetic energy spectrum (dashed line) for three different times for the mechanically forced run. Spectra are shown up to $k = 40$, the maximum wavenumber for which the transfer was analyzed. The maximum wavenumber resolved in the simulation was $k_{max} \approx 85$.

The forced scale [see $Q = 10$ in panel (d)], as described in the beginning of this section, is giving negative magnetic helicity to large scales and positive magnetic helicity to the small scales. This is the largest in amplitude transfer, and is the main source of "absolute" magnetic helicity.

At scales smaller than the energy injection band [see panel (e)], like in the magnetically forced case, (positive) magnetic helicity appears to cascade to smaller scales where it is finally dissipated.

B. Small scale saturated regime

As the amplitude of the magnetic field is increased by dynamo action, the growth of magnetic energy at scales smaller than the forcing band saturates. Meanwhile, the negative peak of the magnetic helicity moves to larger scales [see Fig. 6(a)]. The large scales in the system ($K > 10$) receive (negative) magnetic helicity both locally from slightly smaller scales and non-locally from the forced scales, and give negative magnetic helicity to slightly larger scales if available [see panel (b,c)]. The forced scale [corresponding to $Q = 10$, see panel (d)] gives most of the negative magnetic helicity to the shell where the magnetic helicity spectrum peaks ($K \approx 2$). At the same time, the forced shell gives positive magnetic helicity to slightly smaller scales. Finally, the small scales [panel (e)] cascade the positive magnetic helicity

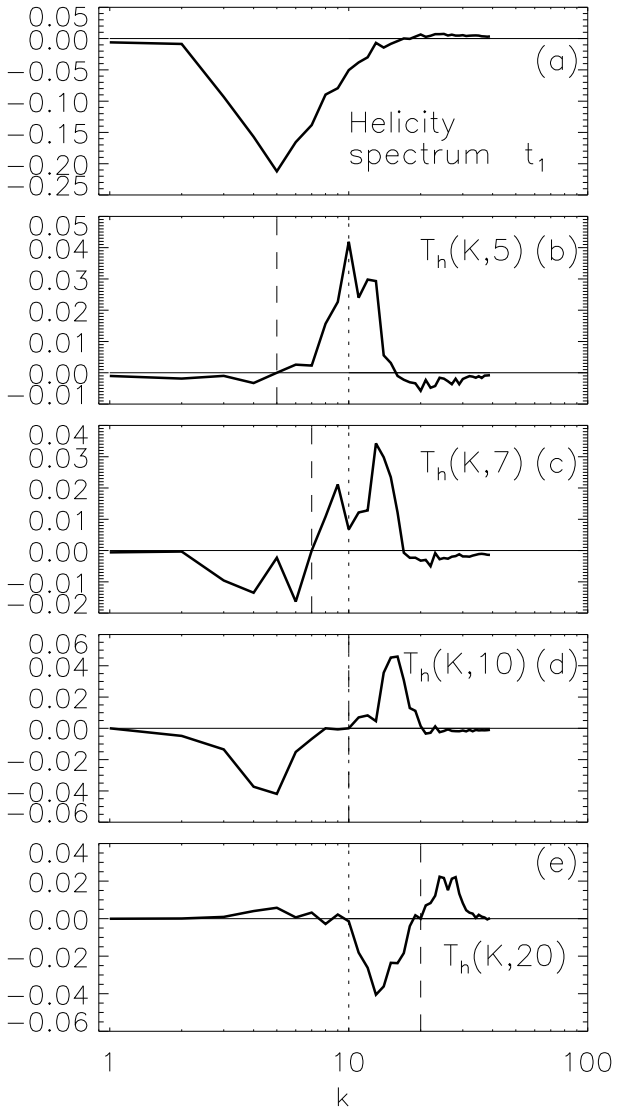

FIG. 5: The spectrum of magnetic helicity (panel a), and transfer of magnetic helicity $\mathcal{T}_h(K, Q)$ normalized by the total magnetic helicity at the shell Q for the mechanically forced run in the kinematic regime. The different panels (b-e) correspond to different values of $Q = 5, 7, 10, 20$. The dashed vertical line indicates the location of the examined value of Q while the dotted line indicates the shell where the system was forced.

to even smaller scales where it is dissipated. In addition, there is a considerable amount of magnetic helicity destruction by transferring positive helicity from the small scales (where the magnetic helicity is mostly positive) directly into the large scales (where helicity is negative, see the positive peak at $K \approx 2$ in panel (e)), decreasing as a result the absolute value of magnetic helicity in both scales. We believe this behavior may be related to reconnection events.

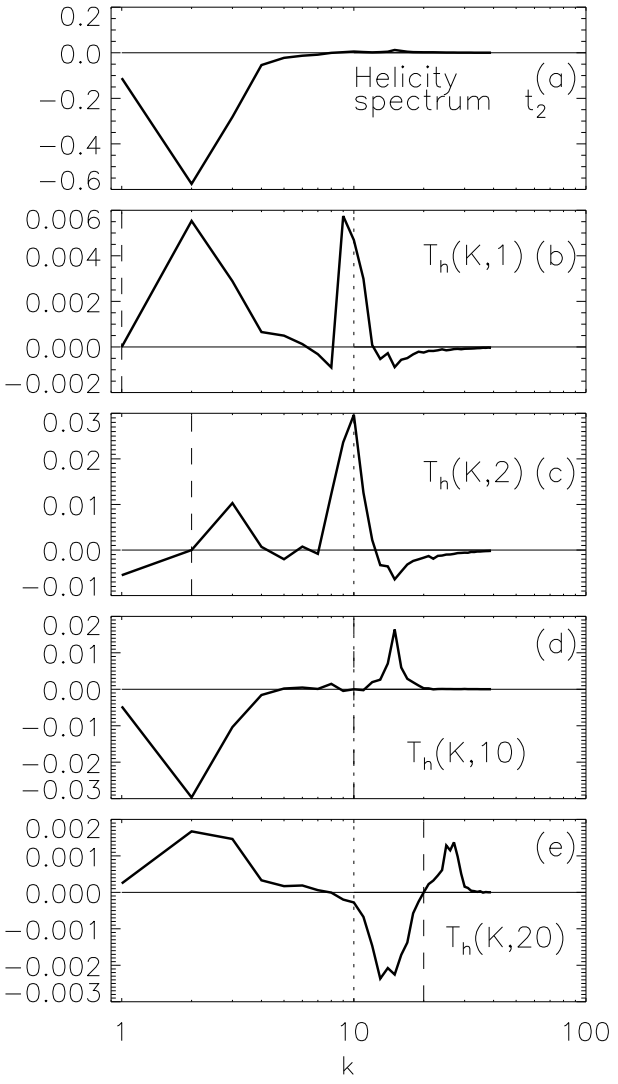

FIG. 6: Magnetic helicity spectrum (panel a) and transfer of magnetic helicity $\mathcal{T}_h(K,Q)$ normalized by the total magnetic helicity in the shell Q, for the mechanically forced run, when the small scales in system are saturated. The different panels (b-e) correspond to different values of $Q = 1, 2, 10, 20$ The dashed vertical line indicates the location of the examined value of Q, while the dotted line indicates the shell where the system was forced.

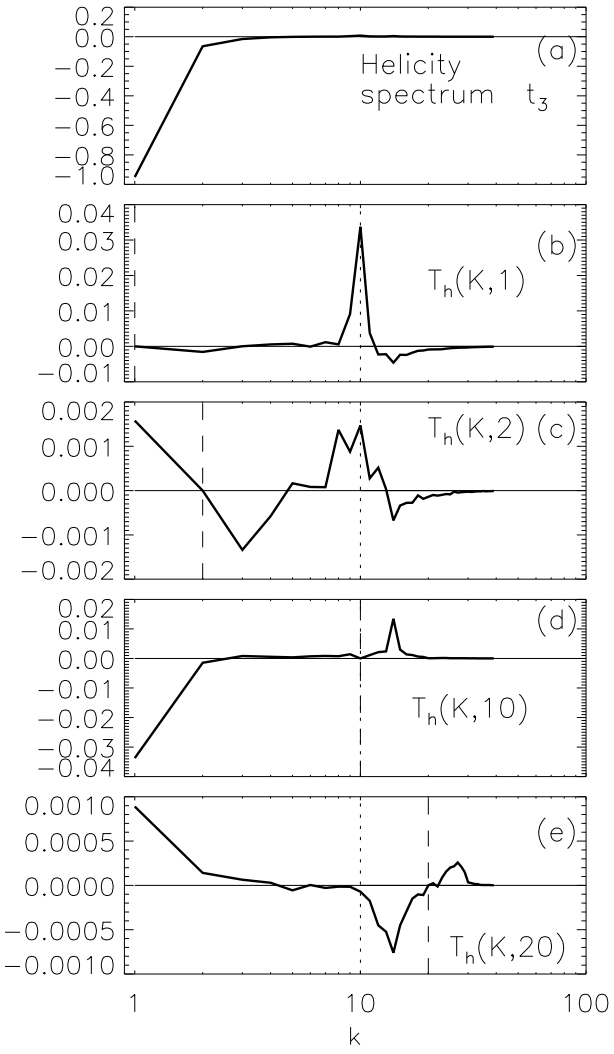

FIG. 7: Magnetic helicity spectrum (a), and transfer of magnetic helicity $\mathcal{T}_h(K,Q)$ (b-e) normalized by the total magnetic helicity in the shell Q, for the mechanically forced run close to the saturation at the large scales. The different panels (b-e) correspond to different values of $Q = 1, 2, 10, 20$. The dashed vertical line indicates the location of the examined value of Q, while the dotted line indicates the shell where the system was forced.

C. Saturated regime

When the system is close to the saturation at all scales, the helicity spectrum peaks at the largest available scale [$K = 1$, see Fig. 7(a)]. At this stage the large scales receive magnetic helicity directly from the forced scales by a non-local process [see panel (b) and (d)]. Such a behavior has also been observed for the transfer of magnetic energy in helical dynamo runs in [18].

In the intermediate scales, between the largest available scale in the box and the forced scale [see Fig. 7(c)], there seems to be a direct cascade of helicity from the large scales to smaller scales. This direct cascade of helicity at large scales is similar to the "reflection" of magnetic helicity at $K = 1$ observed in the magnetically forced run (see Sect. III), and is also also expected to be dependent on the boundary conditions.

The forcing band keeps injecting magnetic helicity of opposite signs at large and small scales [panel (d)], but while positive magnetic helicity is injected at wavenumbers slightly larger than the forcing shell $Q = 10$, most of the negative magnetic helicity is injected non-locally into the shell $K = 1$. Scales smaller than the forced scale [see panel (e)] cascade the positive magnetic helicity to smaller scales where it is dissipated. Again, there is a non local transfer of positive helicity from the small scales to the largest scale (see the positive peak at $K = 1$) leading

to the decrease in the absolute value of the magnetic helicity in both scales. Note that as the result of the inverse cascade of one sign of magnetic helicity at large scales, and the direct cascade of magnetic helicity of the opposite sign at small scales, the system is finally dominated by magnetic helicity of sign opposite to the kinetic helicity injected by the mechanical forcing. This has been observed by Brandenburg [18] and in closures [14].

V. DISCUSSION AND CONCLUSIONS

The results presented above stemming from the two numerical simulations have some important implications that need to be discussed. We start by giving a brief summary of what is observed in the simulations. At the early stages of the evolution of the magnetic field, in both examined runs the peak of the magnetic helicity spectrum appears to be close to the forcing scales although in scales slightly larger. Magnetic helicity inversely cascades in the large scales, both locally by transfer of helicity from the closest neighbor shells, and non-locally by direct transfer from the forced shells. As the systems evolves, the inverse cascade of magnetic helicity leads the magnetic helicity spectrum to peak at the largest available scale in the domain. At this stage, the direct input coming from the non-local transfer of magnetic helicity from the forced scales to the largest attainable scales becomes dominant. At the same time, the local transfer of helicity at intermediate scales changes direction, and magnetic helicity cascades locally to small scales. This direct cascade between the largest scale in the box and the forcing band can be expected to be sensitive to the boundary conditions, and is a non-universal feature common to other systems displaying inverse cascade. Similar behavior has been observed in two dimensional hydrodynamic turbulence [30, 31, 32, 33]. However, we note that the non-local transfer from the forced scales to the large scales is much greater in amplitude than the local direct cascade. This behavior raises the interesting question of which process, the local or non-local cascade, is dominant in open systems like stars or galaxies where no largest available scale can be clearly defined, or where stellar or galactic winds can eject part of the magnetic helicity out of the system.

The small scales behave differently. Unlike the large scales, in the small scales there is a noticeable direct cascade of magnetic helicity to the dissipation scale. This implies that in the limit of infinite Reynolds number in a helically forced flow, there is still going to be at the saturated stage a finite global magnetic helicity, since one sign of magnetic helicity at scales larger than the forced scales will cascade inversely, while the opposite sign of magnetic helicity at small scales will cascade to smaller and smaller scales until it will be dissipated.

It can be argued that this direct cascade of small scale magnetic helicity is counter intuitive (in the sense of self-similarity), since at a given scale the flow does not know if it is at scales smaller than the forcing or larger. It could have been expected therefore to see the same direction of cascade at all scales. This kind of argument however assumes that each scale is completely independent, but this is not the case for MHD. Magnetic helicity in scales larger than the integral scale of a helical flow is generated by the twisting and folding of flux tubes, forcing them to inter-penetrate [34]. At the same time, the twisting causes in small scales the magnetic field lines to spiral around each other, generating small scale magnetic helicity of the opposite sign than that in the large scale. Any further stretching of the flux tube will cause the small scale magnetic helicity (i.e. the twisting of the field lines around the flux tube) to cascade to even smaller scales, even if the large scale helicity is cascading to larger scales. Furthermore, reconnection at small scales changes the topology and the linkage of the field lines at the large scales, and this explains the non-local transfer of helicity from small scales to the large scales, "destroying" in that way the large scale helicity as it is observed in Figs. 6 and 7(e).

We conclude by noting that the overall picture of the cascade of magnetic helicity appears to be more complicated than that of the energy, and crucially depends on the scale and the domain size. Simple assumptions carried over from hydrodynamic turbulence phenomenology do not seem to apply here. Future numerical simulations, experiments and refined theoretical arguments are needed in order to illuminate further the understanding of MHD turbulence and improve the modeling of turbulent flows.

Acknowledgments

Computer time was provided by NCAR. The NSF grant CMG-0327888 at NCAR supported this work in part and is gratefully acknowledged.

[1] G. Glatzmaier and P. Roberts, Science **274**, 1887 (1996).
[2] M. Kono and P. H. Roberts, Rev. Geophys. **40**, 1 (2002).
[3] M. Dikpati and P. Charbonneau, Astrophys. J. **518**, 508 (1999).
[4] D. Nandy and A. R. Choudhuri, Science **296**, 1671 (2002).
[5] P. Bushby and J. Mason, Astronomy & Geophys. **45**, 7 (2004).
[6] A. Shukurov and E. Dormy, *Introduction to galactic dynamos* (Kluwer Acad. Publ., Dordrecht, 2005).
[7] H. K. Moffatt, *Magnetic field generation in electrically conducting fluids* (Cambridge Univ. Press, Cambridge, 1978).
[8] A. D. Gilbert, U. Frisch, and A. Pouquet, Geophys.and

Astrophys. Fluid Mech. **42**, 151 (1988).
[9] C. Nore, M. E. Brachet, H. Politano, and A. Pouquet, Phys. Plasmas Lett. **4**, 1 (1997).
[10] V. Urpin, Phys. Rev. E **65**, 026301 (2002).
[11] M. Steenbeck, F. Krause, and K.-H. Rädler, Z. Naturforsch. **21a**, 369 (1966).
[12] F. Krause and K.-H. Rädler, *Mean-field magnetohydrodynamics and dynamo theory* (Pergamon Press, New York, 1980).
[13] U. Frisch, A. Pouquet, J. Léorat, and A. Mazure, J. Fluid Mech. **68**, 769 (1975).
[14] A. Pouquet, U. Frisch, and J. Léorat, J. Fluid Mech. **77**, 321 (1976).
[15] A. Pouquet and G. S. Patterson, **85**, 305 (1978).
[16] M. Meneguzzi, U. Frisch, and A. Pouquet, Phys. Rev. Lett. **47**, 1060 (1981).
[17] S. Kida, S. Yanase, and J. Mizushima, Phys. Fluids A **3**, 457 (1991).
[18] A. Brandenburg, Astrophys. J. **550**, 824 (2001).
[19] D. O. Gómez and P. D. Mininni, Nonlin. Proc. Geophys. **11**, 619 (2004).
[20] G. Dar, M. Verma, and V. Eswaran, Physica D **157**, 207 (2001).
[21] O. Debliquy, M. Verma, and D. Carati, Phys. Plasmas **12**, 042309 (2005).
[22] A. Alexakis, P. D. Mininni, and A. Pouquet, Phys. Rev. E (2005), in Press.
[23] P. D. Mininni, A. Alexakis, and A. Pouquet, Phys. Rev. E (2005), in Press.
[24] L. Woltjer, Proc. Natl. Acad. Sci. **44**, 489 (1958).
[25] A. N. Wright and M. A. Berger, J. Geophys. Res. **94**, 1295 (1989).
[26] M. A. Berger, J. Geophys. Res. **102**, 2637 (1997).
[27] F. Waleffe, Phys. Fluids A **4**, 350 (1991).
[28] Q. Chen, S. Chen, and G. L. Eyink, Phys. Fluids **15**, 361 (2003).
[29] Q. Chen, S. Chen, G. L. Eyink, and D. D. Holm, Phys. Rev. Lett. **90**, 214503 (2003).
[30] L. M. Smith and V. Yakhot, J. Fluid Mech. **274**, 115 (1994).
[31] V. Borue, Phys. Rev. Lett. **72**, 1475 (1994).
[32] G. Boffetta, A. Celani, and M. Vergassola, Phys. Rev. E **61**, R29 (2000).
[33] S. Danilov and D. Gurarie, Phys. Rev. E **63**, 061208 (2001).
[34] Y. B. Zeldovich, A. A. Ruzmaikin, and D. D. Sokoloff, *Magnetic fields in astrophysics* (Gordon and Breach Science Pub., New York, 1983).
[35] N. Seehafer, Phys. Rev. E **53**, 1283 (1996).